J Electroceram (2010) 24:319–325
DOI 10.1007/s10832-009-9576-9

Synthesis, and measurement of structural and magnetic properties, of $La_{1-x}Cd_xCoO_3$ perovskite ceramic oxides

Manjunath B. Bellakki · Jaydip Das · V. Manivannan

Received: 9 April 2009 / Accepted: 23 April 2009 / Published online: 8 May 2009

Abstract Perovskite-type Cd-doped $LaCoO_3$ materials were synthesized by a simple solution-based combustion process. The synthesized materials were characterized by powder X-ray diffraction (XRD), scanning electron microscopy (SEM), diffuse reflectance (DR) in the UV-VIS, and magnetic property measurements. The parent $LaCoO_3$ compound showed spin-glass transition at low temperatures, and with progressive Cd doping, showed transition to paramagnetic ordering. The changes in magnetic properties of the materials are correlated to the changes in structural features resulting from the Rietveld structural refinement of the materials.

Keywords Oxides · Combustion synthesis · X-ray diffraction · Spin transition

1 Introduction

Perovskite type (ABO_3) cobaltate oxides have attracted interest for many years because of their excellent magnetic, electrical conductivity, catalytic activity, electrochemical, and other properties [1–5]. ABO_3 perovskite oxides have been extensively studied by several researchers as they have applications in catalytic oxidation and combustion, automobile exhaust purification, and sewage treatment. They have also been used in production of environmental catalysts and gas sensors [6–8]. Several methods for synthesis of Perovskite type (ABO_3) cobaltate oxides have been reported in the literature [9–14].

Among transition-metal oxides with the perovskite structure ABO_3, the compound $LaCoO_3$ is of particular interest because it shows a spin-state transition as a function of temperature. $LaCoO_3$ is a nonmagnetic insulator in its ground state. Partial substitution of the trivalent La^{3+} site by divalent metal ions; for example, Ca^{2+}, Ba^{2+}, or Sr^{2+}, results in a change in the oxidation state of Co metal ions, the creation of oxygen vacancies, or both, in order to maintain the charge neutrality of the compound [15–17]. Thus, doped rare-earth cobaltate materials have the potential to exhibit "mixed conductivity" (i.e. a combination of electronic and ionic conductivity). These mixed conductivity materials have been proven to increase the performance of solid oxide fuel cells (SOFC) and therefore have technological importance [7]. The ratio of Co^{3+}/Co^{4+} is an important factor in magnetic phase transition in cobaltates.

Studies on M^{2+} substituted $LaCoO_3$ (where M=Ca, Sr, or Ba) have been reported in the literature [18–20]. Cd is also a divalent metal atom similar to Ca, Ba, and Sr, and Cd-doped materials can exhibit interesting physical phenomenon. Cd-doped $LaMnO_3$ samples were recently shown to exhibit metal-insulator transition properties in addition to the giant magnetoresistance (i.e. >85% drop in resistance at a low magnetic field of 1 Tesla) [21]. We have been motivated to study the effect on the physical properties of $LaCoO_3$ perovskites due to substitution of Cd^{2+}. Such an approach of study, i.e., establishing a structure–property relationship in $La_{1-x}Cd_xCoO_3$ materials, has not been reported so far.

2 Experimental

$La_{1-x}Cd_xCoO_3$ ($0 \leq \times \leq 0.2$) compounds were prepared by dissolving stoichiometric amounts of metal nitrates in a

M. B. Bellakki · J. Das · V. Manivannan (✉)
Department of Mechanical Engineering,
Colorado State University,
Fort Collins, Colorado, USA
e-mail: mani@engr.colostate.edu

V. Manivannan
Department of Chemistry, Colorado State University,
Fort Collins, Colorado, USA

minimum amount of water in a Pyrex dish. A calculated amount of fuel glycine was added. A detailed procedure for calculating the metal nitrates to fuel ratio has been described elsewhere [22, 23]. The resulting aqueous solution was introduced into a muffle furnace maintained at 400°C. The mixture boiled, followed by frothing, and ignited with evolution of a large amount of gases. The mixture ignited and caught fire to give a voluminous combustion product. Assuming complete combustion, the general equation for the formation of samples can be proposed as follows:

$$(1-x)La(NO_3)_3+xCd(NO_3)_2+Co(NO_3)_3+C_2H_5NO_2 \rightarrow La_{1-x}Cd_xCoO_3 + CO_2 + H_2O(g) + N_2(g) \quad (1)$$

The phase purity and crystal structure were examined by a Bruker X-ray diffractometer with a nickel filter using Cu K_α radiation. For Rietveld refinement, data were collected at a scan rate of 0.5°/min with a 0.02°step size for 2θ from 10° to 100°. The data were refined using the Rietveld analysis program, *FullProf* [24]. The morphology of the powder was examined using a JEOL JSM-840A scanning electron microscope fitted with an energy dispersive X-ray analyzer (EDX). The magnetization measurements were performed using a SQUID magnetometer in the temperature range 2.5–300 K with a static applied field of 1,000 Oe. Diffuse reflectance spectra were recorded in the wavelength range 250–2,500 nm using a Varian Associated Cary 500 double beam spectrophotometer. Compressed polytetrafluoroethylene (PTFE) was used for standard calibration (100% reflectance). The ratio of the Co^{3+}/Co^{4+} concentrations was determined by iodometric titration for all the samples [25].

3 Results and discussion

3.1 Structure

Powder XRD patterns of combustion synthesized $La_{1-x}Cd_xCoO_3$ ($0 \le x \le 0.2$) perovskite cobaltates are shown in Fig. 1. All the samples crystallize in single phase, and the product oxide could be indexed in a rhombohedral symmetry having the lattice parameters a=5.438 Å and c= 13.084 Å (hexagonal setting) with space group *R-3c* (No. 167). The structural parameters are refined by the Rietveld method using the *FullProf* program [24]. In Fig. 2, observed, calculated, and difference XRD patterns of the typical refined XRD patterns of (a) $LaCoO_3$ and (b) $La_{0.8}Cd_{0.2}CoO_3$ compounds are given. There is a good agreement between observed and calculated patterns. The refined structural parameters, selected bond lengths, and

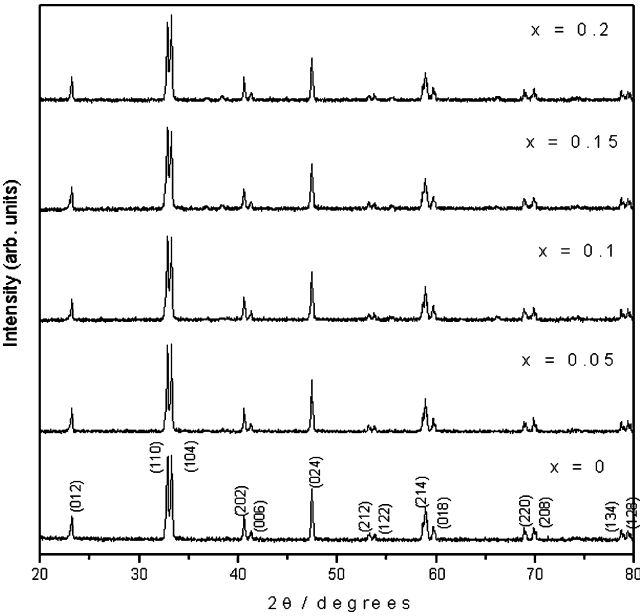

Fig. 1 Powder XRD patterns of $(La_{1-x}Cd_x)CoO_3$ materials

bond angles are summarized for all the samples in Table 1. We tried to synthesize the samples with x>0.2, but the impurity CdO was observed in these phases. We have therefore focused on doping levels of only up to 20% Cd substitution into $LaCoO_3$. The reduction in the lattice parameter leading to unit-volume reduction is due to the substitutional effect of replacing La^{3+} (1.36 Å) ions with similar sized Cd^{2+} (1.31 Å) ions [26].

3.2 Microstructure study

To further understand the structural features of $La_{1-x}Cd_xCoO_3$ ($0 \le \times \le 0.2$) samples, SEM was performed (Fig. 3). Figures 3(a) and b show typical SEM images of parent and 20% Cd-doped $LaCoO_3$ samples. The microstructure showed the particles are sub-micron size and agglomerated, or already connected to each other, resulting in an open or porous structure. EDX in combination with SEM showed the materials synthesized have homogeneous composition.

3.3 Magnetic-property measurements

Figure 4 shows the magnetic susceptibility as a function of temperature for the undoped and various Cd-doped samples. A broad peak at about 75 K followed by a decrease in the susceptibility in the $30 \le T \le 75$ K range for the undoped sample is observed. A sharp Curie-like increase in the magnetic susceptibility in the $5 \le T \le 30$ K range is indicative of the presence of paramagnetic defects or impurities. The overall shape is consistent with the previous reports for the undoped samples. As more Cd is doped into $LaCoO_3$,

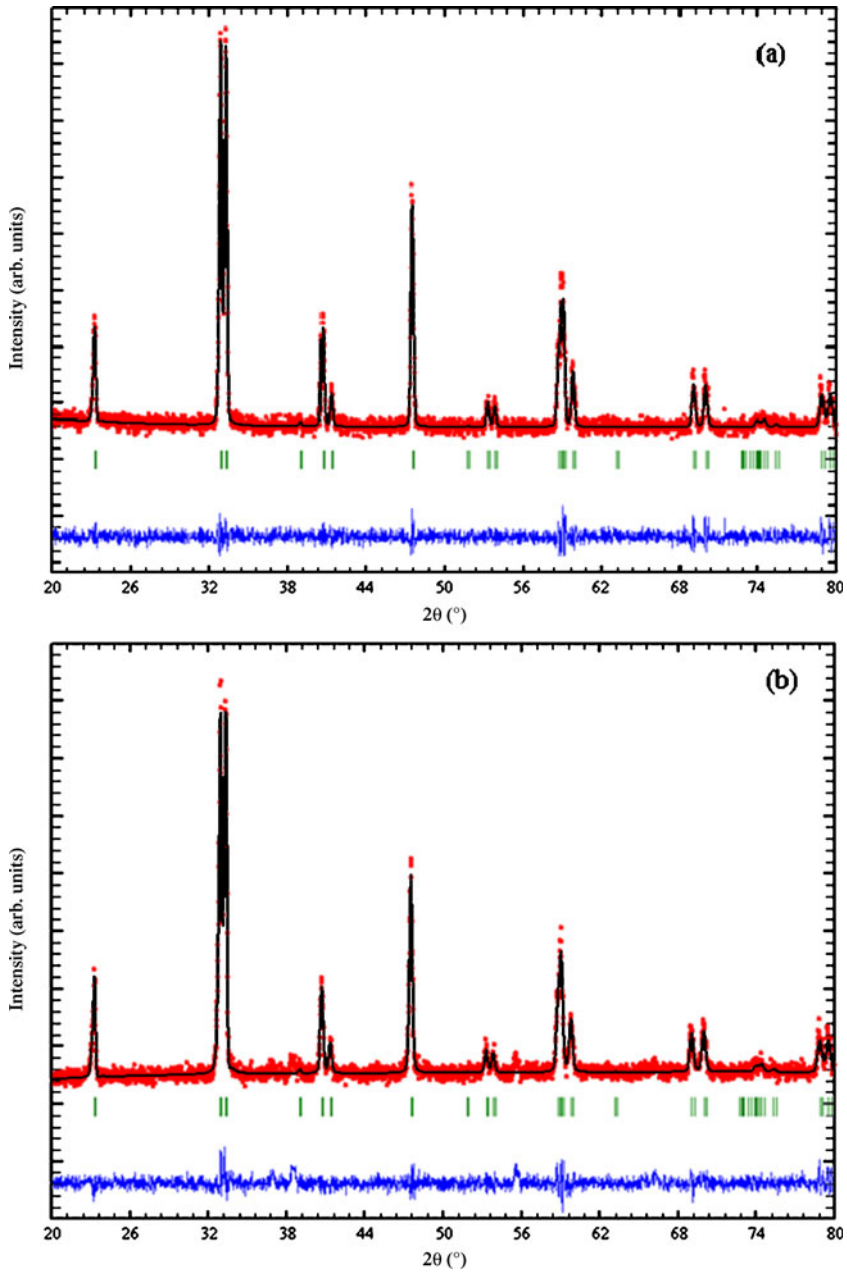

Fig. 2 Typical observed, calculated and difference Rietveld refined XRD patterns of (**a**) $LaCoO_3$, and (**b**) 20% Cd doped $LaCoO_3$ materials

the Curie-like contribution at low temperatures increases. The broad peak could not be observed for x>5%.

3.3.1 Discussion

The susceptibility *vs.* T profiles in the low T regime below 35 K have been fitted to a Curie-Weiss law of form C/(T+θ), where C is the Curie constant (inset of Fig. 4). The inset shows that the Curie constant C increases linearly with dopant concentration. A linear fit has been done and is shown by a solid-line in the figure. The slope of the fit is about 0.024, representing the increase in the Curie constant for each percentage of Cd. Applying the well-known relation for Curie constant:

$$\text{Curie constant } C = N_A g^2 \mu_B^2 S(S+1)/3K_B \quad (2)$$

where N_A is the Avogadro's constant, g is the Lande g factor, μ_B is the Bohr magneton, and K_B is the Boltzmann constant, one obtains a spin S value of about 3/2 for each Cd^{2+} at the La site.

The presence of a Cd^{2+} ion at the La^{3+} site is expected to produce a hole with S=1/2 to the canted antiferromagentic system. If the hole remains free and does not interact with

Table 1 Reitveld refined structural parameters for $La_{1-x}Cd_xCoO_3$ ($0 \leq \times \leq 0.2$) perovskites.

Compounds Crystal System Space group	$LaCoO_3$ Rhombohedral *Rc-167*	$La_{0.95}\ Cd_{0.05}CoO_3$	$La_{0.90}\ Cd_{0.10}CoO_3$	$La_{0.85}\ Cd_{0.15}CoO_3$	$La_{0.80}\ Cd_{0.20}CoO_3$
Lattice parameters					
$a=b$ (Å)	5.438(3)	5.436(2)	5.435(3)	5.433(2)	5.434(6)
c (Å)	13.084(4)	13.082(3)	13.084(4)	13.082(5)	13.086(6)
Cell volume (Å^3)	335.042(4)	334.731(4)	334.706(2)	334.426(5)	334.692(8)
La/Cd	6a				
x	0.0000	0.0000	0.0000	0.0000	0.0000
y	0.0000	0.0000	0.0000	0.0000	0.0000
z	0.2500	0.2500	0.2500	0.2500	0.2500
Co	6b				
x	0.0000	0.0000	0.0000	0.0000	0.0000
y	0.0000	0.0000	0.0000	0.0000	0.0000
z	0.0000	0.0000	0.0000	0.0000	0.0000
O_1	18e				
x	0.4551(2)	0.4568(1)	0.4580(7)	0.4549(5)	0.4537(2)
y	0.0000	0.0000	0.0000	0.0000	0.0000
z	0.2500	0.2500	0.2500	0.2500	0.2500
R-factors (%)					
R_P	3.98	4.54	4.63	4.37	4.78
R_{WP}	5.68	5.79	5.86	5.55	6.16
R_{Bragg}	2.01	1.97	3.68	2.95	5.08
R_F	2.05	2.14	3.76	3.49	4.78
Bond lengths (Å)					
Co-O	1.9267(2)	1.9251(3)	1.9242(2)	1.9247(4)	1.9240(6)
Bond angles (°)					
Co-O-Co	165.440(4)	165.987(3)	166.374(5)	165.380(6)	164.995(5)

the cobalt spins that are anti-ferromagnetically aligned, it is expected to add a Curie-like behavior to the magnetic susceptibility of the parent systems. The main graph in Fig. 3 indeed showed an increase in the Curie contribution in magnetic susceptibility with dopant concentrations at low temperatures. However, from the analysis of the Curie constant *vs.* Cd concentrations, the value of the free spin S=3/2 is about three times higher than the S=1/2 expected for each Cd. In other words, it suggests that each Cd is responsible for three spins instead of one spin.

If one considers a picture where Cd is not replacing the La and instead is responsible for creating a vacancy at the La^{3+} site, the formula becomes slightly non-stoichiometric and can be viewed as $La_{1-x}\square_xCoO_3$ (□—vacancy) and the deficiency in each of the La^{3+} ions will introduce three effective free spins to the system. This effective spin supposedly contributes to the magnetic properties and is responsible for the increase in the Curie-like behavior at low temperatures.

The substitution of Cd^{2+} into $LaCoO_3$ introduces a cation charge deficiency in the system which can be compensated by a) creation of mixed valency (Co^{3+}–Co^{4+}), b) creation of oxygen vacancies, and c) an ionic radii effect at A site leading to creation of a vacancy at La site. .In addition, a combination of a) and b) is also possible, as demonstrated in $SrFeO_{3-x}$ materials synthesized in air [27]. Authors of literature on $La_{0.7-x}\square_xSr_{0.3}CoO_3$ materials showed that, in general, the samples are oxygen substoichiometric, and the portion of substoichiometric O_2 increases with increasing La-deficiency and creation of vacancies at La sites, leading to a gradual decrease of the unit cell volume and accounts for the observed spin-glass to paramagnetic and ferromagnetic magnetic behavior as a result of the progressive increase in deficiency [28]. The observed magnetic properties in our samples (S=3/2), attributed to the effective spins of a vacancy created at the La^{3+} site, are consistent with such observations.

Rietveld refinement showed that with progressive Cd doping, the length of the Co-O bond showed a decreasing trend. The bond length decreased from 1.9267 Å at x=0 to 1.9240 Å at x=0.2. The Co-O-Co bond angle remains almost constant (Table 1). The structural parameters

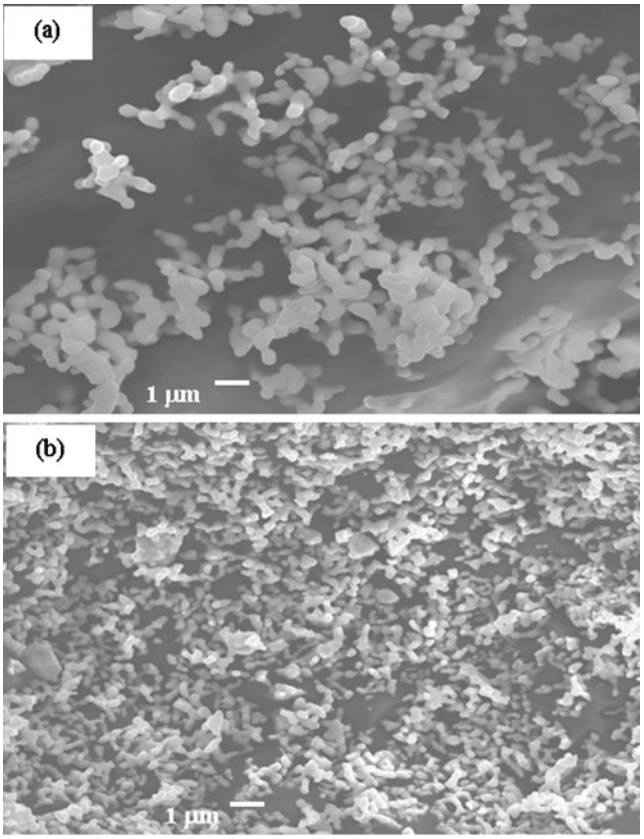

Fig. 3 Scanning electron micrographs of (**a**) $LaCoO_3$, and (**b**) 20% Cd doped $LaCoO_3$ materials

obtained for the parent compound are consistent with the literature [29]. The parent compound exhibits a spin-glass behavior at low temperature which originates due to the competition between the ferromagnetic (Co^{3+}–O–Co^{4+}) and the antiferromagnetic (Co^{3+}–O–Co^{3+} and Co^{3+}–O–Co^{4+}) interactions [28]. Chemical titrations showed the portion of Co^{4+} increased from 3.5% at 0% doping to 14.9% at 20% Cd doping. With increasing Cd doping, the contribution of effective spins at the La^{3+} vacancy is more pronounced, leading to the observed paramagnetic behavior.

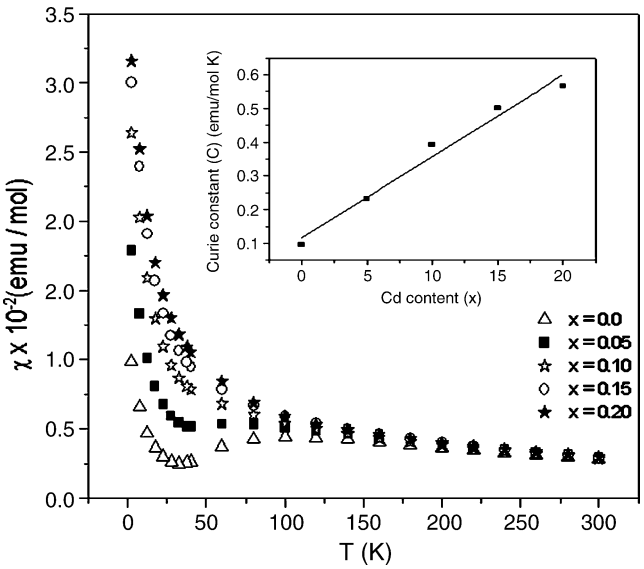

Fig. 4 Magnetic susceptibility (χ) vs. temperature at a magnetic field of 1,000 Oe for (La, Cd)CoO_3 materials (inset figure shows the plot of Curie constant for various Cd substituted $LaCoO_3$ materials)

3.4 UV-vis diffuse reflectance spectroscopy

Recently it was shown that nanocrystals of $LaCoO_3$ materials have promise for their catalytic behavior, decreasing the decomposition temperature up to 130°C and improving the burning rate [30]. Also, it was shown that perovskite type oxides exhibit higher photocatalytic activity compared to the currently standard TiO_2 materials under visible radiation [31]. One reason for TiO_2's low efficiency

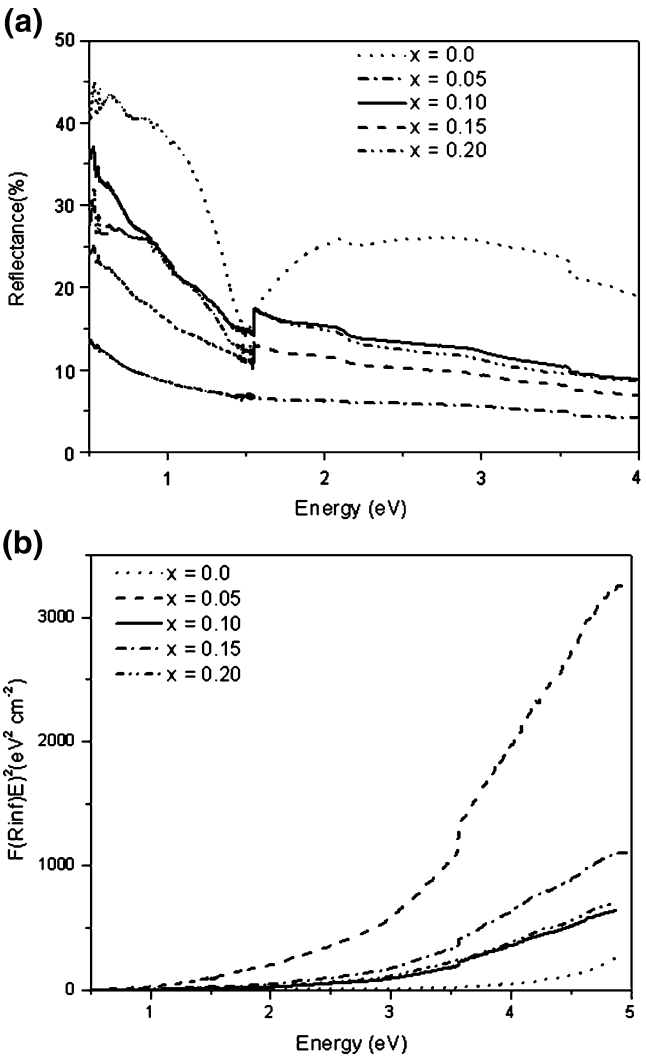

Fig. 5 (**a**) Diffuse reflectance spectra and (**b**) Plot of $F(R_\infty)$ vs. E(eV) for the estimation of the optical absorption edge energy of (La, Cd) CoO_3 perovskite materials

in utilizing the solar spectrum is the wide band gap of 3.2 eV, and accordingly, low band gap materials are preferred. In this regard, it is relevant to explore Cd-doped $LaCoO_3$ perovskties for such applications by determining the optical band-gap of the materials. To measure the optical band gap of $La_{1-x}Cd_xCoO_3$ ($0 \leq x \leq 0.2$), DR measurements were carried out (Fig. 5). Figure 5(a) shows the diffuse reflectance spectra of $La_{1-x}Cd_xCoO_3$ ($0 \leq x \leq 0.2$) samples in the UV-vis-NIR range. The diffuse reflectance data was used to calculate the absorption coefficient from the Kubelka-Munk [32, 33] (KM) function defined as:

$$F(R_\infty) = \alpha/S = (1 - R_\infty)^2 \Big/ 2\,R_\infty \quad \text{where} \quad R_\infty = R_{\text{sample}}/R_{\text{PTCO}} \tag{3}$$

Here α is the absorption coefficient, S is the scattering coefficient, and $F(R_\infty)$ is the KM function. The energy dependence of the material in the UV-vis-NIR was further explored. The energy dependence of semiconductors near the absorption edge is expressed as:

$$\alpha E = K\left(E - E_g\right)^\eta \tag{4}$$

Here E is the incident photon energy ($h\nu$), E_g is the optical absorption edge energy, K is a constant, and the exponent η is dependent on the type of optical transition as a result of photon absorption [34]. The exponent η is assigned a value of 1/2, 3/2, 2, and 3 for direct allowed, direct forbidden, indirect allowed, and indirect forbidden transition, respectively [35].

For the diffused reflectance spectra, the KM function can be used instead of α for estimation of the optical absorption edge energy [34]. It was observed that a plot of $F(R_\infty)$ E vs. E was linear near the edge for direct allowed transition ($\eta = 1/2$). The intercept of the line on the abscissa ($F(R_\infty)$ $E=0$) gave the value of the optical absorption edge energy. The values determined for the parent compound are in agreement with literature values [36]. The corresponding values for the Cd substituted samples (0.05, 0.1, 0.15 and 0.2) are 2.55±0.2, 2.94±0.2, 2.75±0.2, and 2.53±0.2 eV respectively. Figure 5(b) shows the plot of the same. The changes are indicative of the creation of energy states within the band gap of the material, and with increasing Cd doping the doped states broaden in to a band overlapping with the O 2p band [37]. The low band gap values indicate these materials can have higher photocatalytic activity compared to the TiO_2 standard materials which have poor photocatalytic efficiency due to their wide band gaps (~3.2 eV) [38]. The diffuse reflectance spectra for direct band gap orthorhombic (β) Ta_2O_5 prepared by heating Ta metal in air, are also recorded for comparison [39]. The value of optical absorption edge energy for the indirect allowed transition for Ta_2O_5 was found to be 4.0±0.2 eV, which is consistent with those seen for the β-Ta_2O_5 reported [40]. The low band-gap of the materials can be attractive for photo catalytic applications due to the favorable band-structure of these perovskite oxides.

4 Conclusions

We have successfully synthesized novel (La, Cd)CoO_3 materials by a simple solution-based combustion process, and determined the structural parameters and extent of solid-solubility by detailed Rietveld structural refinement. The magnetic property studies show that with progressive Cd doping, the cobaltite undergoes phase transition from spin-glass to paramagnetic behavior which could be due to the contribution of the effective spins of vacancies at La^{3+} sites. Optical property measurements showed that the high optical band-gap nature of the parent compound transition to narrow band-gap materials (~2.5 eV) and position them for potential photocatalytic applications.

Acknowledgements One of the authors would like to thank Prof. Allan Kirkpatrick, Head of Department, Department of Mechanical Engineering, Colorado State University for his continued help, support and assistance.

References

1. J.W. Stevenson, T.R. Armstrong, R.D. Carnein, L.D. Pederson, W. J. Weba, J. Electrochem. Soc. **143**, 2722 (1996). doi:10.1149/1.1837098
2. M. Cherry, M.S. Islam, C.R.A. Catlow, J. Solid State Chem. **118**, 125 (1995). doi:10.1006/jssc.1995.1320
3. H. Kusaba, G. Sakai, K. Shimanone, N. Minura, N. Yamazoe, Solid State Ionics **52–153**, 689 (2002)
4. N. Miura, H. Murae, H. Kusaba, J. Tamaki, G. Sakai, N. Yamazoe, J. Electrochem. Soc. **146**, 2581 (1999). doi:10.1149/1.1391975
5. L.G. Tejuca, J.L.G. Fierro (eds), *Properties and applications of perovskite-type oxides* (Marcel Dekker, New York, 1993)
6. E. Traversa, S. Villanti, G. Gusmano, H. Aono, Y. Sadaka, J. Am. Ceram. Soc. **82**, 2442 (1999)
7. K. Huang, H.Y. Lee, J.B. Goodenough, J. Electrochem. Soc. **145**, 3220 (1999). doi:10.1149/1.1838789
8. F.J. Kahn, P.S. Pershan, J.P. Remeika, Phys. Rev. Lett. **186**, 891 (1969)
9. C.N.R. Rao, J. Gopalakrishnan, *New directions in solid state chemistry*, 2nd edn. (Cambridge University Press, Cambridge, 1997)
10. A.R. West, *Solid state chemistry and its applications* (Wiley, New York, 1984)
11. C.N.R. Rao, Mater. Sci. Eng. B **18**, 1 (1993). doi:10.1016/0921-5107(93)90109-Z. and references therein
12. A.K. Cheetam, P. Day, *Solid state chemistry techniques* (Oxford University Press, Oxford, 1987)
13. M. Rajendran, A.K. Bhattacharya, J. Eur. Ceram. Soc. **26**, 3675 (2006). doi:10.1016/j.jeurceramsoc.2006.01.008
14. X. Qi, J. Zhou, Z. Yue, Z. Gui, Z. Yue, Z. Gui, L. Li, Mater. Chem. Phys. **78**, 25 (2002). doi:10.1016/S0254-0584(02)00341-3

15. A. Ben Amor, M. Koubaa, W. Cheikhrouhou-Koubaa, A. Cheikhrouhou, J. Alloy. Comp. **467**, 78 (2009). doi:10.1016/j.jallcom.2007.12.030
16. N. Orlovskaya, M. Lugovy, S. Pathak, D. Steinmetz, J. Lloyd, L. Fegely, M. Radoyic, E.A. Payzant, E. Lara-Curzio, L.F. Allard, J. Kuebler, J. Power Sources **182**, 230 (2008). doi:10.1016/j.jpowsour.2008.03.072
17. M. Koubaa, W. Cheikhrouhou-Koubaa, A. Cheikhrouhou, L. Ranno, Physica B **403**, 4012 (2008). doi:10.1016/j.physb.2008.07.044
18. M.A. Senaris-Rodriguez, J.B. Goodenough, J. Solid State Chem. **118**, 323 (1995). doi:10.1006/jssc.1995.1351
19. M. Kriener, C. Zobel, A. Reichl, J. Baier, M. Cwik, K. Berggold, H. Kieerspel, O. Zabara, A. Freimuth, T. Lorentz, Phys. Rev. B **69**, 094417 (2004). doi:10.1103/PhysRevB.69.094417
20. A. Chainani, M. Mathew, D.D. Sharma, Phys. Rev. B **46**, 9976 (1992). doi:10.1103/PhysRevB.46.9976
21. M. Sahana, M.S. Hegde, N.Y. Vasanthacharya, V. Prasad, S.V. Subramanyam, Appl. Phys. Lett **18**, 2701 (1997). doi:10.1063/1.120182
22. K.C. Patil, S.T. Aruna, S. Ekambaram, Curr. Opin. Solid State Mater. Sci. **2**, 158 (1997). doi:10.1016/S1359-0286(97)80060-5
23. K.C. Patil, Bull. Mater. Sci. **16**, 533 (1993). doi:10.1007/BF02757654
24. D.B. Wiles, R.A. Young, J. Appl. Cryst. **14**, 149 (1981). doi:10.1107/S0021889881008996
25. R.N. Singh, C. Shivakumara, N.Y. Vasanthacharya, S. Subramanian, M.S. Hegde, S. Rajagopal, A. Sequeira, J. Solid State Chem. **137**, 9 (1998). doi:10.1006/jssc.1997.7653
26. R.D. Shannon, Acta Crystallogr. A **32**, 751 (1976). doi:10.1107/S0567739476001551
27. H. Yamamura, H. Handeda, S. Shirasaki, K. Takada, J. Solid State Chem. **36**, 1 (1981). doi:10.1016/0022-4596(81)90185-7
28. A. Ben Amor, M. Koubaa, W. Cheikhrouhou-Koubaa, A. Cheikhrouhou, J. Alloy. Comp. **457**, 1 (2008). doi:10.1016/j.jallcom.2007.02.118
29. C. Zhang, B.H. Kim, J.S. Kim, Y.W. Park, Phys. Lett. A **348**, 58 (2005). doi:10.1016/j.physleta.2005.07.088
30. Y. Wang, X. Yang, L. Lu, X. Wang, Thermochim. Acta **443**, 225 (2006). doi:10.1016/j.tca.2006.01.030
31. L. Shudan, J. Liqiang, F. Wei, Y. Libin, X. Baifu, F. Honggang, Mater. Res. Bull. **42**, 203 (2007). doi:10.1016/j.materresbull.2006.06.010
32. P. Kubelka, F. Munk, J. Tech. Phys. **12**, 593 (1931)
33. G. Kortum, *Reflectance spectroscopy principles, methods, applications* (Springer-Verlag, New York, 1969)
34. D.G. Barton, M. Shtein, R.D. Wilson, S.L. Soled, E. Iglesia, J. Phys. Chem. B **34**, 630 (1999). doi:10.1021/jp983555d
35. J. Tauc, R. Grigorov, A. Vancu, Phys. Status Solidi **15**, 627 (1966). doi:10.1002/pssb.19660150224
36. T. Arima, Y. Tokura, J.B. Torrance, Phys. Rev. B **48**, 17006 (1993). doi:10.1103/PhysRevB.48.17006
37. D.D. Sharma, A. Chainani, R. Cimino, P. Sen, C. Carbone, M. Mathew, W. Gudat, Europhys. Lett. **15**, 513 (1992). doi:10.1209/0295-5075/19/6/012
38. M.R. Hoffman, S.T. Martin, W. Choi, W. Bahnemann, Chem. Rev. **95**, 69 (1995). doi:10.1021/cr00033a004
39. B.R. Sahu, L. Kleinman, Phys. Rev. B **69**, 165202 (2004). doi:10.1103/PhysRevB.69.165202
40. W.H. Knausenberger, R.N. Tauber, J. Electrochem. Soc. **120**, 927 (1973). doi:10.1149/1.2403602